



The RED Fouling Monitor: A novel tool for fouling analysis

E.J. Bodner^{a,b}, M. Saakes^a, T. Sleutels^a, C.J.N. Buisman^{a,b}, H.V.M. Hamelers^{a,*}

^a Wetsus, European Centre of Excellence for Sustainable Water Technology, Oostergoweg 9, 8911 MA Leeuwarden, the Netherlands

^b Department of Environmental Technology, Wageningen University, Bornse Weilanden 9, 6708 WG Wageningen, the Netherlands



ARTICLE INFO

Keywords:

Salinity gradient
RED Fouling Monitor
Fouling analysis
Organic fouling
Ion-exchange membranes

ABSTRACT

RED is a technology for harvesting energy using the salinity gradient between river (RW) and seawater (SW). Membrane fouling can decrease the net power density. Fouling inhibition might be indispensable. For implementing antifouling strategies more detailed insights upon fouling are required. In RED stacks investigations of single membranes are practically impossible. We introduce the RED Fouling Monitor, in which one side of a single ion-exchange membrane in contact to a foulant-containing feed stream can be studied under OCV and current conditions. Fouling is detectable in four configurations: (1) SW/AEM, (2) RW/AEM, (3) SW/CEM and (4) RW/CEM. Functionality is provided by a novel flow-through salt bridge enabling ionic connection and the incorporation of reference electrodes in close proximity to the membrane surface. The results indicate a stable, reproducible performance under un-fouled conditions. Upon SDBS exposure RW/AEM fouling showed a more pronounced fouling response than SW/AEM fouling. Fouling is partly attributable to the current density and the current field direction. An irreversible, internal fouling of the AEM is indicated when exposed to SDBS in SW. RW/AEM fouling shows to be reversible. With prospect to future systematic investigations this tool can be used to test various configurational, operational designs, different pre-treatment schemes and the fouling potential of feed streams at different seasons. This will result in valuable insights for new constructional sites for future RED plants.

1. Introduction

Reverse electrodialysis (RED) is a promising technology for the production of renewable energy from the controlled mixing of river and seawater [1]. The difference in the chemical potential of these two solutions is the driving force for the RED process [2]. The concentrated (seawater) and diluted solutions (river water) are separated by an alternating series of anion- and cation-exchange membranes. Anions are transported in the direction of the anode through anion-exchange membranes (AEM) and cations are transported towards the cathode through cation-exchange membranes (CEM). This separation of charge in the ionic current is converted into an electrical current by a (reversible) redox reaction at the electrodes [1–3].

One of the most severe problems within many membrane-based technologies is the phenomenon of fouling [4]. It has been established that fouling could be a major drawback for RED applications under environmental conditions, dramatically decreasing the effective net power density output and hindering a long-term sustainable energy generation [5]. Major operational parameters affected by fouling include the increase of the feed channel pressure drop, the increase in electrical resistance (ohmic and non-ohmic) and the decrease of the

open circuit voltage (OCV) that is generated by the salinity gradient over an ion-exchange membrane, which in itself is directly affected by changes in the membrane permselectivity. Changes in these parameters ultimately affect the overall RED performance in terms of net power density and may endanger the long-term applicability of RED for a sustainable power generation [5,6].

Contrary to pressure-driven membrane applications, energy intensive pre-treatment schemes and hazardous chemical cleaning regimes for fouling inhibition are inconceivable and not favored for RED purposes. This is attributable to a required positive net power output and the fact that the total water flow has to be directly discharged into the environment. When comparing RED to various membrane-based technologies, unique characteristics are identifiable. Compared to pressure-driven membrane systems, in RED water hardly permeates the ion-exchange membrane but flows along the membrane [7]. Compared to conventional pressure-driven membranes systems in RED systems different module (stack) designs, hydrodynamic conditions and different membrane materials are used. Similar to RED, in electrodialysis (ED) and electrodialysis reversal (EDR) an alternating pile of ion-exchange membranes is stacked between two electrodes. However, different inter-membrane distances and higher current densities are used

* Corresponding author.

E-mail address: bert.hamelers@wetusus.nl (H.V.M. Hamelers).

[[8–10,17]]. In ED/EDR a single feed is desalinated by applying an electrical potential difference, while in RED energy is obtained using the difference in chemical potential of two individual feed water inputs [11]. Due to the named technological differences, the understanding of the fouling behavior within different membrane-based technologies cannot completely be transferred to RED applications.

In previous RED related studies, the issue of fouling has been addressed and few possible mitigation strategies have been tested under both laboratory and pilot scale conditions [6,21,22,24]. However, up to date fouling investigations are commonly based on trial and error approaches, while detailed insights in the specific type of fouling and the mode of action upon the RED performance have not been studied in great detail. Detailed insights about the possible interaction of different fouling types, the membrane-foulant interaction and the possible contribution of current-related fouling are sparse. This not only highlights the complexity of fouling, but also underlines the importance for more detailed RED fouling studies.

This research gap might be attributable to the adverse configurational circumstances of a conventional RED stack, making a representative and detail-rich fouling investigation essentially difficult, whereas the relatively small inter-membrane distances [17] make an in-situ inspection practically impossible. In RED two different types of ion-exchange membranes are used: cation- and anion-exchange membranes. Both sides of each membrane are subjected to natural waters containing foulants: sea- and river water. Due to the differences in membrane type and the general compositional differences of river- and seawater the following four different fouling constellations can be expected to occur in a single RED stack: (1) seawater/AEM, (2) river water/AEM, (3) seawater/CEM and (4) river water/CEM. This makes a specific and distinctive fouling analysis essentially difficult. Furthermore, when applied under natural conditions, the progression of fouling-relevant electrochemical and/or hydrodynamical operational parameters is a rather cumulative and in-differential output of various factors. For a more distinctive fouling analysis the six-compartment cell [12] as a dynamic fouling analysis tool for a single ion-exchange membrane could be helpful. However, in comparison to a RED stack, the compartment thickness is rather large and the use of membrane spacers is not possible [12]. In previous studies it has been shown, that hydrodynamic conditions, flow distributions and different spacer designs play a significant role in fouling development [13,14]. Thus, using the six-compartment cell, representative fouling conditions cannot be mimicked for RED purposes. Various membrane related fouling studies rely on the implementation of the so-called membrane fouling simulator (MFS) [15]. Nevertheless, the MFS is used for pressure-driven membrane process, whereas not applicable for monitoring the current-driven RED process using ion-exchange membranes.

Apparently, there is a lack of suitable tools available offering a detailed, defined, representative, non-destructive, real-time fouling analysis for RED applications. The objective of this study was to develop a tool able of doing so, the RED Fouling Monitor. A tool capable of following the progression of fouling-relevant operational parameters for one side of a single ion-exchange membrane (either CEM or AEM) in contact to a single feed water stream (either sea or river water) under both OCV and current conditions.

2. Materials and methods

2.1. Configuration of the RED Fouling Monitor

For the configuration of the RED Fouling Monitor a cross-flow RED stack provided by REDstack BV, the Netherlands was used and separated at our laboratory into two half-stacks (HS₁ and HS₂, see Fig. 1). Similar to the principle of voltaic and galvanic electrochemical half-cells, one half-stack facilitates the oxidation-reaction at the anode while the second half-stack facilitates the reduction-reaction at the cathode. A salt bridge typically enables the ionic connection between two half-

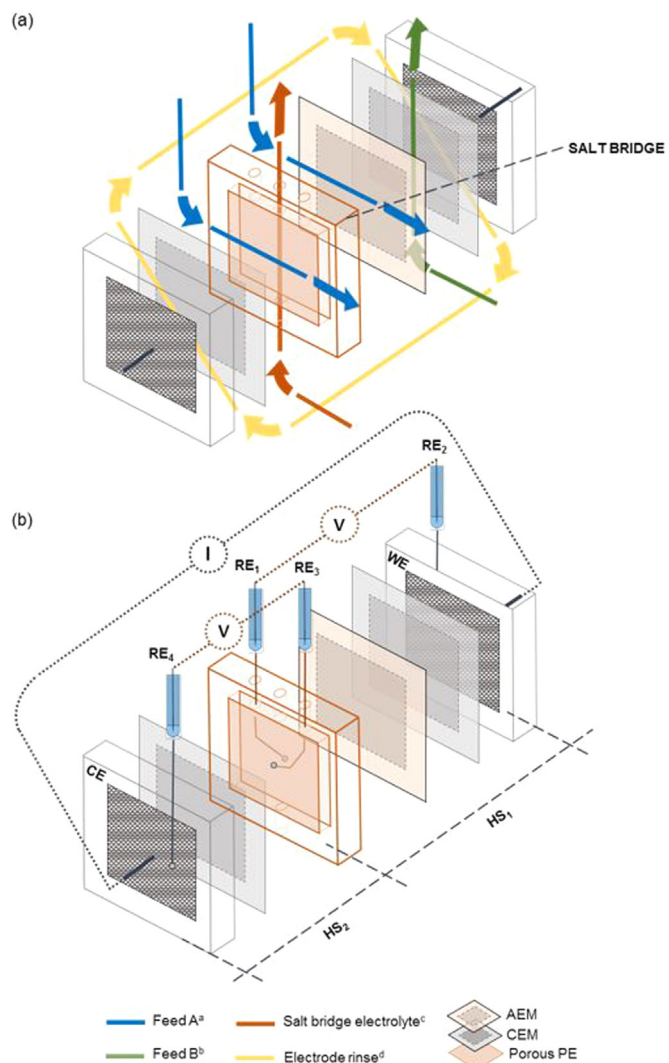


Fig. 1. General configuration of the RED Fouling Monitor, both half-stacks (HS₁ and HS₂) include a Pt-coated Ti-mesh electrode, the flow-through salt bridge has an exposed area of $10 \times 10 \text{ cm}^2$, closed at both sides with a pre-treated agar-filled porous PE, the flow-through salt bridge uses the same salt concentration as the surrounding media, the thickness of the flow-through salt bridge is 30 mm, (a) feed stream distribution in cross-flow configuration, one cell-pair consisting of a CEM, and an AEM + a closing CEM, gasket-integrated spacers are not shown, depending on the experiment membrane-spacer systems and ^{a,b,c,d} are freely variable, (b) electrochemical connections, the salt bridge has two installed Ag/AgCl reference electrodes (RE) to measure the voltage difference across the reference electrodes, current density (I) is controlled between working (WE) and counter electrode (CE), the potential response (V) is measured for half-stack 1 (HS₁) between reference electrode 1 (RE₁) and RE₂ and/or for HS₂ between RE₃ and RE₄.

cells. Each half-stack is equipped with a meshed platinum-coated ($2.5 \mu\text{m}$) titanium electrode provided by Magneto Special Anodes BV, The Netherlands. Both electrodes, shown in Fig. 1 as WE (working electrode) and the CE (counter electrode) acting as either anode or cathode have the same active area of $10 \times 10 \text{ cm}$. For the anolyte and catholyte rinse, a solution of $0.05 \text{ M K}_4\text{Fe}(\text{CN})_6$, $0.05 \text{ M K}_3\text{Fe}(\text{CN})_6$ with a bulk solution of 0.25 M NaCl was used to facilitate the redox reaction. Both $\text{K}_4\text{Fe}(\text{CN})_6$ and $\text{K}_3\text{Fe}(\text{CN})_6$ were purchased from Sigma-Aldrich Chemie GmbH (Steinheim, Germany). The electrode rinse solution was continuously re-circulated into the electrode compartments at a flow rate of 150 ml/min using a peristaltic pump (Cole-Parmer, Masterflex L/S Digital drive 116 USA). An overpressure of 0.3 bar was applied to avoid bulging of the feed water compartments and to ensure proper

membrane and spacer packing. To prevent electrolyte leakage into the feed water compartment the electrode compartments were closed and shielded using cation-exchange membranes (standard grade, CMX-fg, Neosepta) provided by ASTOM Corporation, Tokyo and 50 μm thick silicone gaskets. As anion-exchange membrane the standard Type 1 membrane provided by Fujifilm BV (Tilburg, The Netherlands) was used. To accommodate both sea- and river water compartments and separate the ion-exchange membranes extruded gasket-integrated spacers of 330 μm thickness (Deukum GmbH, Germany) are introduced (not shown in Fig. 1). Depending on the required experiment, the membrane and/or spacer type, the number of cell pairs is freely adjustable.

The ionic connection is given by the incorporation of a homemade dynamic flow-through salt bridge. The flow-through salt bridge consists of a poly (methyl methacrylate) (PMMA) frame (PyraSied Xtreme Acrylic BV, The Netherlands) with an open area of 10×10 cm and a thickness of 25 mm. Transport of the electrolyte solution into the surrounding media is diminished upon separation using 2.5 mm thick pre-treated sintered, porous polyethylene (PE) sheets with a median pore size of 35 μm (POREX Technologies GmbH, Germany) for both sides of the flow-through salt bridge.

To ensure ionic connection and stable operation, the porous PE sheets are pre-treated and filled with 3% (m/v) BBL Agar Grade A (melting point between 80 and 90 $^{\circ}\text{C}$) obtained from Becton, Dickinson and Company (New Jersey, United States) using a vacuum oven (BINDER GmbH) at 90 $^{\circ}\text{C}$ for 30 min. The PE-sheets have a stable temperature resistance within the range from 0 to 100 $^{\circ}\text{C}$ and were thus not damaged during this procedure. Depending on the media considered as the surrounding bulk, the ionic strength and composition of the agar was adjusted accordingly to either 0.5 M (artificial seawater) or 0.017 M (artificial river water) using sodium chloride (NaCl). NaCl (technical grade, 99.5% purity) was provided by ESCO, The Netherlands. For all solutions de-mineralized water was used as solvent. Before insertion into the RED Fouling monitor, the pre-treated porous PE sheets were cooled down to room temperature and stored in either artificial sea- or river water. To prevent electrolyte leakage, the PMMA frame and corresponding porous PE sheets are sealed using 50 μm thick silicone gaskets. Contrary to typical static salt bridges used for electrochemical purposes, the flow-through salt bridge is equipped with individual in- and outlets enabling a continuous renewal of fresh electrolyte solution, ensuring ionic connection and stable operation. To further lower the impact of diffusion of ions from or to the salt bridge or osmotic water transport, the ionic strength of the electrolyte solution inside the salt bridge is chosen identical to the surrounding media (artificial sea- or river water).

The spatial separation of both half-stacks of the cross-flow stack enables the incorporation of reference electrode-systems (RE-systems) (Fig. 1b). Each RE-system consists of an independent single junction Ag/AgCl 3 M KCl reference electrode (QiS, ProSense BV, The Netherlands) submerged into a closed beaker attached to a Haber-Luggin capillary containing a solution of either 0.5 or 0.017 M NaCl, depending on what solution surrounds the flow-through salt bridge. The tip of the capillary is directly integrated into the PE sheet facing the surrounding media and bringing the sensing point of the RE (RE₁ and RE₃) in close proximity to the ion-exchange membrane under investigation. Bringing the sensing point in close proximity investigative site follows the same principal and concept as the six-compartment cell, a common tool for determining inter alia electrical resistances of ion-exchange membranes [12]. Furthermore, this configuration ensures the reference electrodes and the electrochemical measurements to be independent to any possible changes attributable to the electrolyte solution inside the flow-through salt bridge. Since the RE do not directly interfere with the water flow (hydrodynamic conditions) and the electrical field experimental representativity with regard to conventional RED stacks is given. Single junction Ag/AgCl 3 M KCl reference electrodes (QiS, ProSense BV, The Netherlands) are inserted into the inlets of both

anolyte and catholyte to enable the electrochemical measurements of HS₁ and HS₂. A detailed illustration is given in Fig. 1.

Using a single RED Fouling Monitor in the configuration as shown in Fig. 1 it is theoretically possible to follow two out of four fouling constellations at the same time (river water/AEM, river water/CEM). Presumed, the media directly surrounding the salt bridge is river water (0.017 M NaCl) containing the foulant and the second feed stream only contains sodium chloride in a corresponding concentration (0.5 M NaCl). By using a second identically constructed RED Fouling Monitor with opposite polarization the fouling constellations sea water/AEM, sea water/CEM can be followed. Lies the area of interest in only one out the four possible fouling constellations, analogously electrochemical measurements can be adjusted and performed either between RE₁ and RE₂ or between RE₃ and RE₄. Due to the specific position of RE₁ and RE₃ and their independency of the electrolyte solution of the salt bridge their function cannot be merged.

2.2. Organic fouling investigation using the RED Fouling Monitor

2.2.1. Feed waters

As feed solutions of sodium chloride, resembling artificial sea- and river water, were used. The seawater had a concentration of 0.5 M and river water had a concentration of 0.017 M. NaCl (technical grade, 99.5% purity) was provided by ESCO, The Netherlands. To ensure complete salt dissolution and room temperature equilibration the feed waters were prepared at least 24 h before the experiment. During the experiment the RED Fouling monitor was continuously fed by both solutions using a cross flow-velocity of 1 cm/s adjusted by peristaltic pumps (Cole-Parmer, Masterflex L/S Digital drive 116 USA).

2.2.2. Organic model foulant

In order to test the developed RED Fouling Monitor and to gain further insights about organic fouling within RED systems two separate organic fouling experiments were conducted. In the first experiment the model foulant was subjected to river water and a single side of an anion-exchange membrane, while during the second experiment the anion-exchange membrane was exposed to the foulant present in the seawater. Natural waters like sea- and river water often both contain negatively charged organic compounds (e.g. humic acids) [5,21,25]^{*}. In this study sodium dodecyl benzene sulfonate (SDBS), a negatively charged organic surfactant not commonly found in natural waters, was used as the model organic fouling compound. This compound was chosen, because in previous ED organic fouling studies SDBS showed to interfere with charged groups of anion-exchange membranes within a relatively short time period, whereas a long time period is required to observe the fouling impact of humic acids. [16]. Furthermore, humic acids typically are a mixture of complex substances and less defined in their composition [21,25]. The main focus in this study lies in the introduction of the RED Fouling Monitor to the scientific community and the overall proof of principle. Therefore a compound having a relatively fast, defined and straight forward fouling response was favored. Depending on the experiment and as further explained in the following paragraph SDBS was added to either artificial sea- or river water to reach a final concentration of 750 mg/l (Fig. 2, Table 1). SDBS containing feed water was continuously fed to the RED Fouling monitor at a cross flow velocity of 1 cm/s using a peristaltic pump (Cole-Parmer, Masterflex L/S Digital drive 116 USA). During both experiments the foulant was individually subjected to one side of a single anion-exchange membrane (Fuji Type 1), whereas the remaining compartments were continuously kept under un-fouled conditions and fed by artificial sea- or river water (Fig. 2).

2.2.3. Experimental design

During the fouling experiments a fixed sequence of conditions was followed (Table 1). Baseline measurements (condition A) as shown in Table 1 were conducted to show the performance of the RED Fouling

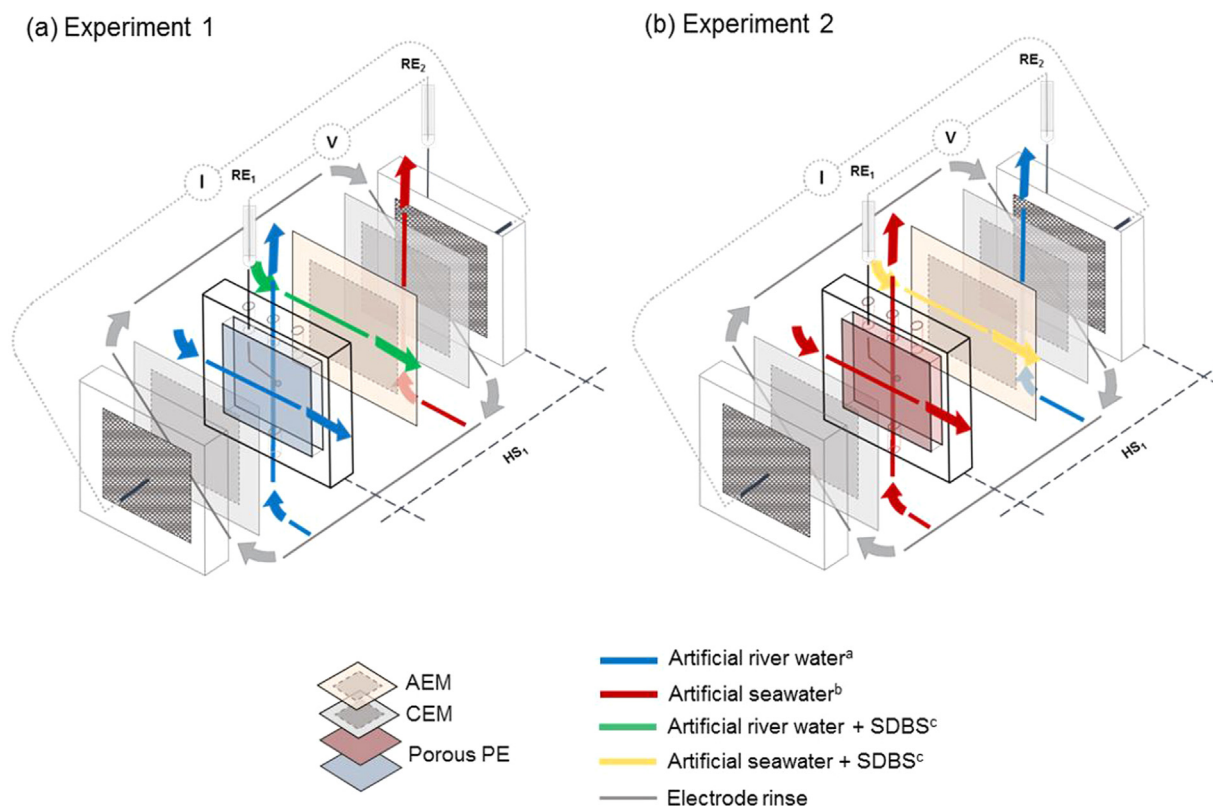


Fig. 2. General experimental design and flow distribution during organic fouling experiments using the RED Fouling Monitor, ^aartificial river water = 0.017 M NaCl, ^bartificial seawater = 0.5 M NaCl and ^cSDBS (= 750 mg/l) as the organic foulant, the current (I) is controlled between outer electrodes, the potential (V) is measured for half-stack 1 (HS₁) between reference electrode 1 (RE₁) and RE₂, OCV and electrical resistance are continuously logged in loops following a stage of OCV (120 s) and a subsequent current density step (600 s) under four conditions: (1) baseline conditions: 7.5 A/m², no SDBS added, (2) fouling conditions: continuous dosing of SDBS, 7.5 A/m², (3) fouling conditions: continuous dosing of SDBS, 15 A/m², (4) un-fouled condition, 7.5 A/m², no SDBS added, (a) experiment 1, investigated fouling constellation: river water/AEM, (b) experiment 2, investigated fouling constellation: seawater/AEM.

Table 1

Sequence of conditions followed during fouling experiments.

Experiment #	Condition A	Condition B	Condition C	Condition D
1 ^a	Baseline ^c $J = 7.5 \text{ A/m}^2$	Fouling ^d $J = 7.5 \text{ A/m}^2$	Fouling ^d $J = 15 \text{ A/m}^2$	Un-fouled ^e $J = 7.5 \text{ A/m}^2$
2 ^b	Baseline ^c $J = 7.5 \text{ A/m}^2$	Fouling ^d $J = 7.5 \text{ A/m}^2$	Fouling ^d $J = 15 \text{ A/m}^2$	Un-fouled ^e $J = 7.5 \text{ A/m}^2$

^a Investigated fouling constellation: river water/AEM.

^b Investigated fouling constellation; seawater/AEM.

^c Un-fouled conditions using plainly artificial feed waters, no SDBS added.

^d Continuous dosing of SDBS (750 mg/l) to one side of a single AEM (Type 1, Fujifilm).

^e No SDBS dosed.

Monitor under un-fouled conditions. In experiment 1 the fouling effect of SDBS in the river water on the anion-exchange membrane was investigated. In experiment 2 the focus was on studying the impact of SDBS present in the seawater on the anion-exchange membrane. By adjusting to condition B the system is continuously subjected to SDBS, while keeping the same constant current density of 7.5 A/m². During condition C the current density is doubled to see the impact of extended current levels, while during condition D the system is fed with pure artificial waters and a constant current density of 7.5 A/m² to investigate the irreversible impact of fouling. The current densities were chosen to fit previously reported levels typically used in RED [10].

2.2.4. Electrochemical measurements

All measurements were performed using the IviumStat. XRe (Ivium Technologies BV, the Netherlands) with a compliance up to $\pm 2 \text{ A/}$

$\pm 50 \text{ V}$ connected to both the working (WE) and counter electrode (CE) of the RED Fouling Monitor (Fig. 1b). The electrochemical measurements were conducted in a configuration in which the RE-systems were individually connected to a peripheral differential amplifier (PDA) (Ivium Technologies BV, the Netherlands). Electrochemical measurements were run and logged using IviumSoft (Ivium Technologies BV, the Netherlands). Using this configuration the current (I) of the RED Fouling Monitor can be controlled between the counter (CE) and the working electrode (WE), whereas the potential response (V) is measured between the targeted reference electrodes (RE₁-RE₂ and/or RE₃-RE₄). In the experiments performed in this paper fouling is studied with respect to the anion-exchange membrane, thus the potential between RE₁ and RE₂ of half-stack 1 (HS₁) is followed (Fig. 2).

The applied electrochemical measurements comprised of different chronopotentiometrical stages (Fig. 3) applied during different conditions (Table 1). The RED Fouling Monitor was run in alternating steps of constant current density (7.5 A/m²) for 600 s and OCV for 120 s (Fig. 3). After 150–180 min, respectively the constant current density was doubled to reach 15 A/m² (Table 1).

During each stage of OCV and constant current density both the open potential ($E_{\text{OCV, RE}_1\text{-RE}_2}$) and potential response $E_{J, \text{RE}_1\text{-RE}_2}$ under current conditions were logged after reaching steady state potentials. Subsequently, the electrical resistance $R_{\text{RE}_1\text{-RE}_2}$ between RE₁ and RE₂ of HS₁ can be derived according to Ohms law [5] as follows:

$$R_{\text{HS}_1} = R_{\text{RE}_1\text{-RE}_2} = R_{\text{ohmic}} + R_{\text{non-ohmic}} = \frac{\Delta E_{\text{RE}_1\text{-RE}_2}}{J_{\text{WE-CE}}} \\ = \frac{E_{\text{OCV, RE}_1\text{-RE}_2} - E_{J, \text{RE}_1\text{-RE}_2}}{J_{\text{WE-CE}}} \quad (1)$$

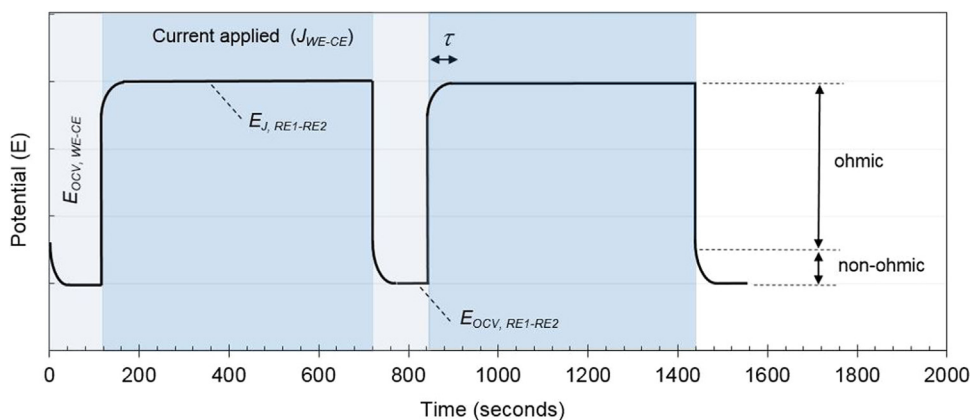


Fig. 3. Illustration of electrochemical measurements performed during experiments 1 and 2, in which the RED Fouling Monitor is run in OCV ($E_{OCV, WE-CE}$) for 120 s and subsequently subjected to a constant current density (J_{WE-CE}) of either 7.5 or 15 A/m² for 600 s, measurements are looped during the entire experimental duration, the open circuit potential ($E_{OCV, RE1-RE2}$) and the potential response under current conditions ($E_{J, RE1-RE2}$) for half-stack 1 (HS₁) is measured in between two individually connected reference electrodes (RE₁ and RE₂), the ohmic potential response is defined as the ohmic resistance multiplied by the applied current density ($R_{ohmic} \cdot J$), the non-ohmic is defined by the time response until a steady state voltage is reached

is presented as τ .

In which $R_{RE1-RE2}$ is the total electrical area resistance ($\Omega \text{ cm}^2$) measured between RE₁ and RE₂ of half-stack 1 (R_{HS1}). The total resistance is subdivided into ohmic (R_{ohmic}) and non-ohmic ($R_{non-ohmic}$) electrical resistances. $\Delta E_{RE1-RE2}$ (V) represents the potential difference derived from the $E_{OCV, RE1-RE2}$ (V) and the potential $E_{J, RE1-RE2}$ (V) during current density conditions J_{WE-CE} (A/m²). $E_{J, RE1-RE2}$ represents the measured potential between RE₁ and RE₂ under current conditions in which J_{WE-CE} is the overall controlled current density of either 7.5 or 15 A/m².

3. Results and discussion

In this study we introduce the RED Fouling Monitor, a novel tool for a detailed fouling analysis for RED purposes. The operational applicability is studied under both un-fouled and organically fouled conditions using SDBS, and different fouling behaviors are highlighted, underlining the RED fouling complexity and the need for further detailed RED fouling investigations using the introduced RED Fouling Monitor.

3.1. Operational performance

Prior to the fouling investigations the operational stability was tested using artificial feed waters in two different configurations, in which either river or seawater is chosen to act as the salt bridge electrolyte solution and the surrounding media (Fig. 4). In both cases the RED Fouling Monitor was continuously controlled at a constant current

density of 7.5 A/m². The potential difference showed a stable progression for 600 s, in which the potential response for the case of Fig. 4b is smaller due to the increased salinity of the electrolyte solution (seawater). The obtained results highlight the operational stability of the novel flow-through salt bridge.

The electrical resistance and the OCV both represent appropriate operational performance parameters for a RED related fouling analysis [5,6,22]. In Fig. 5 both OCV and area resistances are plotted for two fouling experiments over the complete experimental duration measured for HS₁ in between RE₁ and RE₂ (Fig. 2). The experimental design and applied conditions follow the pattern introduced in Table 1.

Similar to the stability measurements during baseline measurements (condition A) both experiments show a stable OCV and area resistance measured in between two individual incorporated reference electrodes (RE₁ and RE₂) brought into close proximity to the ion-exchange membrane within an operational cross-flow RED stack. The results during condition A not only show a stable progression under un-fouled, OCV and current density conditions of 7.5 A/m² when run with artificial feed waters, which highlight the stability for the centerpiece of the RED Fouling Monitor, the flow-through salt bridge. The flow-through salt bridge assures the ionic connection under both OCV and constant current conditions, whereat ultimately enables the technological viability of the RED Fouling Monitor. To the best of our knowledge the theoretical principle and technological realization of a flow-through salt bridge with incorporated reference electrodes positioned in the current field is novel to the field of membrane sciences.

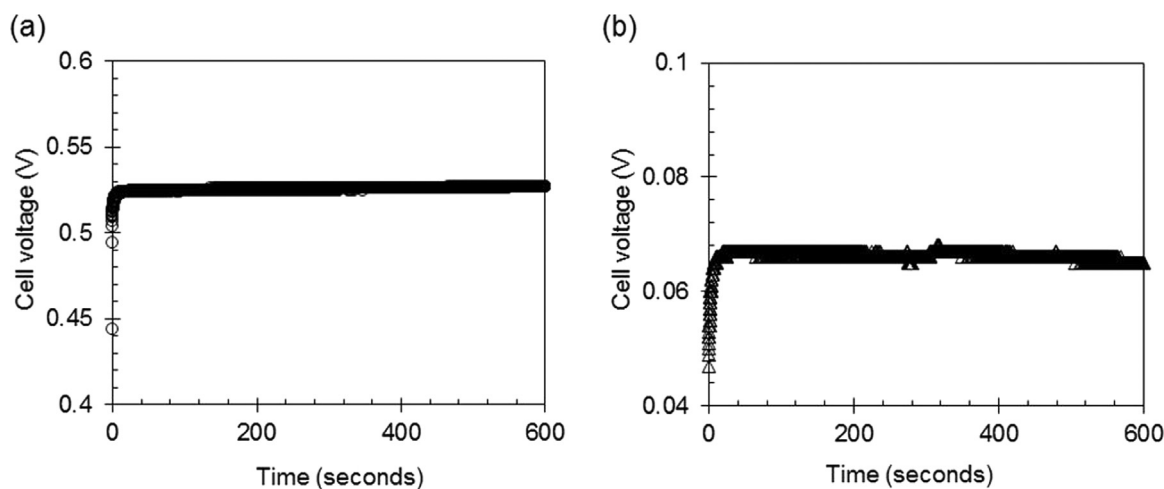


Fig. 4. Stability measurements performed using the RED Fouling Monitor in which the flow-through salt bridge and the surrounding membranes are either subjected to artificial (a) river (0.017 M NaCl) or (b) artificial seawater (0.5 M NaCl), the results represent the potential response under constant current conditions (7.5 A/m²) measured in between the working electrode and the counter electrode, membranes used: CEM (standard grade, CMX-fg, Neosepta), standard Type 1 AEM (Fujifilm).

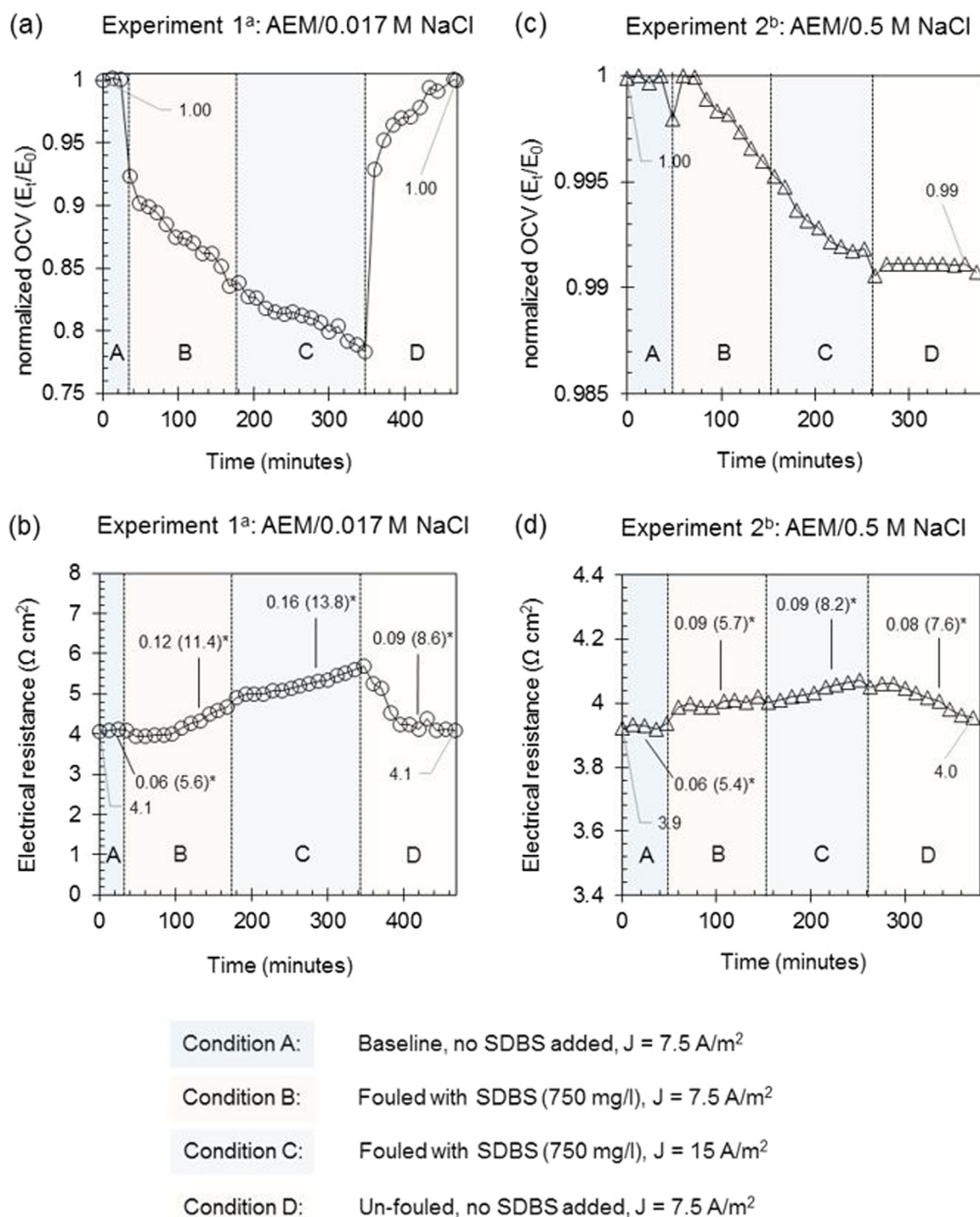


Fig. 5. Normalized OCV and electrical resistances plotted over two fouling experiments measured for half-stack 1 of the RED Fouling Monitor in between two individual reference electrodes (RE_1 - RE_2), membranes used: CEM (standard grade, CMX-fg, Neosepta), standard Type 1 AEM (Fujifilm), during each experiment one side of a single AEM is subjected to SDBS, ^afouling constellation: river water (0.017 M)/AEM, ^bfouling constellation: seawater (0.5 M NaCl)/AEM, during the experiments conditions A-D were applied, electrochemical measurements were performed in loops including a step of OCV (120 s) and a subsequent constant current density of either 7.5 or 15 A/m^2 for 600 s, plotted values were logged and calculated when steady state voltages were established, *values represent the ratio of the non-ohmic to the ohmic resistance, values in brackets show the percentage of the non-ohmic resistance to the total resistance in %.

As soon as the systems are subjected to SDBS (condition B), the OCV is decreased and the electrical resistance is increased, continuously. Evidently, this effect is more pronounced for the case of river water/AEM fouling (OCV loss $\approx 17\%$), whereas less significant in terms of sea water/AEM fouling (OCV loss $\approx 0.5\%$). During the immediate transit from condition A to B a significant sudden drop in OCV ($\approx 10\%$) and electrical resistance (visible, but not significant) is notable in

experiment 1. This drop is attributable to the sudden change of the surrounding media including SDBS, an anionic surfactant and minor differences in temperature ($\pm 0.5^\circ\text{C}$). In aqueous solution SDBS dissociates into a positively charged cation (Na^+) and a negatively charged DBS anion [16]. Due to this addition the electrical conductivity of the aqueous solution increases, thus in terms of experiment 1 both the OCV and electrical resistance are expected to drop. The ratio of

added SDBS to the ionic strength (NaCl) of the artificial feed waters is far smaller with regard to seawater. This explains the significantly lower impact on the apparent electrical conductivity, its sudden impact upon the OCV and the measured electrical resistance during the transit from condition A to B for experiment 2. The apparent sudden drop in OCV and the increase in the electrical resistance for experiment 2 is not attributable to the change in surrounding media but caused by simple short-time pump malfunction.

Evidently, the RED fouling monitor is capable of detecting immediate performance changes in real-time, attributable to an organic foulant, subjected to a single feed water compartment and one side of a single anion-exchange membrane. This further highlights the systems sensitivity and the functionality to act as a helpful fouling detection and analysis tool for RED purposes.

Upon applying condition C the constant current density is doubled from 7.5 A/m^2 to 15 A/m^2 to identify possible changes in the fouling behavior. In Fig. 5b and d it is evident, that the increased current density level changed the fouling related progression of the electrical resistance. Interestingly, the slope in electrical resistance decreased in experiment 1 (Fig. 5b), whereas slightly increased in experiment 2 (Fig. 5d). It is assumed, that this effect is attributable to the opposed direction of current (Fig. 6). In both experiments the negatively charged DBS is attracted by the electrostatic interaction of the positively charged anion-exchange membrane. With regard to experiment 1 the anionic DBS present in the river water is attracted by the anion-exchange membrane, whereas repelled by the current field (Fig. 6a). In contrary, in experiment 2, in which DBS is present in the seawater, both forces favor fouling and DBS to be transported towards the anion-exchange membrane (Fig. 6b). During OCV no added force (current) is applied to assist the movement of charged compounds, therefore the change in progression upon current density increase is less noticeable during OCV (Fig. 5a and c).

In the transition from condition C to D by which the systems are not continuously exposed to the organic foulant (SDBS) anymore the OCV of experiment 1 shows a sudden increase ($\approx 14.5\%$), similarly to the sudden drop during the transition from condition A to B. With respect to experiment 1 both the OCV and electrical resistance tend to go back to its starting point, showing a complete reversible nature of fouling. In contrary, during experiment 2 a relatively small portion of OCV ($\approx 1\%$) is lost and the electrical resistance is slightly increased (not significant). This suggests a more irreversible and internal organic fouling of the anion-exchange membrane probably attributable to the fouling favorable current field direction.

Furthermore, it was possible to differentiate between non-ohmic

and ohmic resistances (Fig. 5b and d). In general, the ohmic resistance can be determined during the sudden jump in potential when an electrical current is applied. The non-ohmic resistance is associated to the concentration change in the boundary layer, which in RED can be defined when a steady state voltage is reached (Fig. 3). The sum of both ohmic and non-ohmic resistances gives the total resistance. Both ohmic and non-ohmic resistances tend to change when ion-exchange membranes are fouled. More generally said, in RED the ohmic component can be attributed to the membrane resistance and the feed water resistance, whereas the non-ohmic resistance is associated with concentration change in the boundary layer. It has also been confirmed, that organic foulants are capable of counterbalancing charged groups of ion-exchange membranes thus increasing the ohmic resistance [5,16,18–20].

Looking at the obtained ratios of non-ohmic to ohmic resistances it is evident that the ohmic resistances dominate the non-ohmic resistances in all cases (Fig. 5b and d). As can be seen, the ratios of the non-ohmic to the ohmic resistances have a similar starting point of 0.06 for both experiments (condition A). During SDBS exposure (condition B), experiment 1 results in a higher ratio of non-ohmic to ohmic resistance (0.12) and a higher total percentage of the non-ohmic resistance (11.4%) in comparison to experiment 2, which shows a total non-ohmic resistance proportion of 5.7% and a non-ohmic to ohmic resistance ratio of 0.09. The same trend is noticeable upon current density increase during condition C. Apparently, during experiment 1 the non-ohmic resistance shows a higher susceptibility towards fouling, whereas during experiment 2 the change in the non-ohmic resistance is relatively lower. The applied current entails ions to be transported towards and through the ion-exchange membrane from the concentrated seawater to the more diluted river water side. Nevertheless, during experiment 2 the driving force for DBS anion transport through or inside the anion-exchange membrane is favored by the current field direction and the electrostatic membrane attraction (Fig. 6b), while in experiment 1 the only driving force for fouling is the electrostatic attraction of the anion-exchange membrane itself (Fig. 6a). The results indicate a better transport of negatively charged ions through or inside the anion-exchange membrane when SDBS is present in the seawater. This ultimately results in a smaller diffusive concentration boundary layer and a relative lower ohmic-resistance. During experiment 1 the negatively charged DBS anions are repelled by the current field. DBS anions are not forced to pass or interact with the anion-exchange membrane by the current field, whereas results in a more superficial electrostatic membrane interaction (Fig. 6). Apparently, this leads to the build-up of a concentration boundary layer and the subsequent

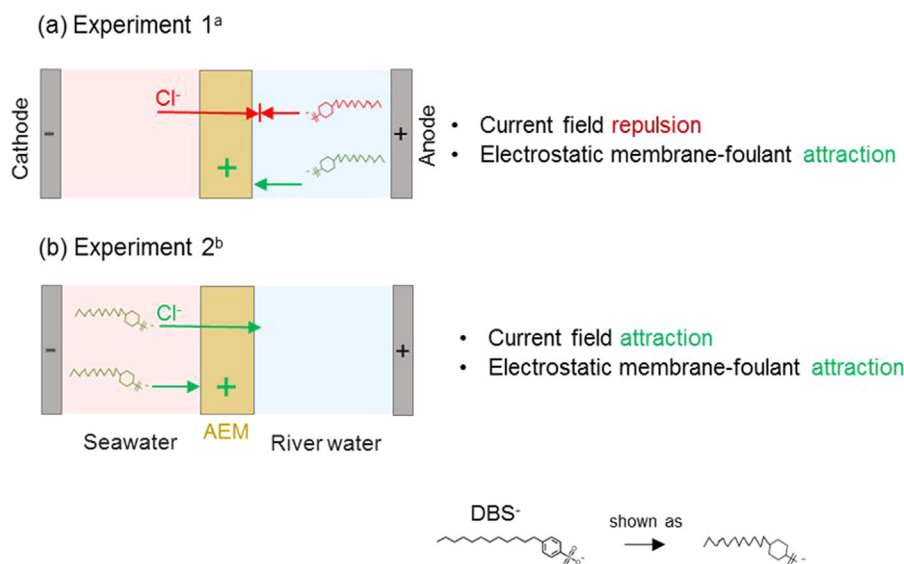


Fig. 6. Illustration of the (electrostatic) interactions of SDBS with the anion-exchange membrane and the current field direction for experiment 1 and 2, (a) represents fouling constellation river water/AEM, SDBS added to artificial river water (b) illustrates the fouling constellation of seawater/AEM, SDBS added to artificial seawater.

increase of non-ohmic resistances even at higher current density levels.

Experiments 1 and 2 were performed independently. Two RED Fouling Monitors were constructed in the same configuration with the same types of ion-exchange membranes (Fig. 2) from the same production run. The experiments were performed with same initial starting conditions (see Section 2.2). The progression of OCV and electrical resistance of HS₁ was followed (Fig. 5). The results show (i) a stable performance and (ii) similar starting points during the applied condition A. Here, it must be clarified that the normalization for the experiments is based upon the same starting point for E₀. The normalized OCV values are plotted to show immediate percentage changes in their progression. The electrical resistances of HS₁ for experiment 1 and 2 both show comparable values of around 4 Ω cm² during un-fouled conditions (condition A). The experimental reproducibility is further highlighted when comparing the initial ratios of non-ohmic resistances to ohmic resistances and of non-ohmic resistances to total resistances expressed in percentages (%). It can be concluded that during condition A the results can be reproduced. A second issue concerns the intrinsic variability of the fouling process. This needs to be investigated and highlighted in future experiments at different experimental conditions with different foulants. In this research it was shown that different fouling constellations can be identified using the RED Fouling Monitor.

3.2. Capabilities of the RED Fouling Monitor

As experimentally shown, the RED Fouling Monitor is capable of following fouling-relevant operational performance parameters in real time, thus detecting detailed differences in fouling behavior. Further insights gained using the RED Fouling Monitor might eventually result in a deepened understanding of RED fouling.

Due to the configurational characteristics, the RED Fouling Monitor is capable of monitoring fouling on one side of a single ion-exchange membrane. This configuration enables to distinguish between the fouling behavior of four possible combinations of membrane and types of water ((1) seawater/AEM, (2) river water/AEM, (3) seawater/CEM and (4) river water/CEM). As the fouling behavior results from the interaction of a specific membrane and type of water we refer to such combination as a fouling constellation. Such distinction is not possible in a RED stack as a specific membrane is exposed always to two types of water. Upon proper membrane handling and foulant extraction various analytical tools could be used for a further fouling quantification.

When run in parallel four fouling constellations can be distinguished experimentally (Fig. 7a). This of course implies the need and preparation for artificial waters simultaneously fed to the RED Fouling Monitor. By connecting inlets and outlets to a differential pressure meter the pressure drop as a measure for colloidal and/or biofouling can be measured and investigated in time. Consequently, when run in parallel the RED Fouling Monitor enables a systematic fouling study, possibly identifying key parameters affecting fouling in RED applications (Fig. 7a). Next to operational parameters this comprises parameters such as the spacer design (thickness, porosity, shape, material), the membrane design (thickness, coating, material, charge), hydrodynamic conditions (cross flow velocities), foulant species present in the feed waters, hybrid systems (profiled membranes, conductive spacers, etc.). Using the parallel application mode novel operational hybrid systems, such as the breathing cell introduced by Moreno et al. [22] or environmentally compatible cleaning regimes such as air-sparging [21] or CO₂-sparging [6] can be studied in more detail (Fig. 7b). Evidently, a broad configurational variety of commercially available and newly developed products can be tested and optimized using the RED Fouling monitor to find solutions less susceptible towards fouling.

In contrast to the MFS [15] fouling can be studied under both open circuit and current conditions. Due to a broad variety of possible charged foulant species (e.g. humic acids, clay particles, etc.) to be possibly affected by a current field the hypothesis for a current related fouling within ion-exchange membrane-based system appears obvious.

This is further emphasized with the obtained results (Fig. 5) and highlighted by organic fouling studies performed on ED under different current density conditions [23]. Using the RED Fouling Monitor the question for current related fouling could be further highlighted and investigated. The applicability of the RED Fouling Monitor under both current and OCV conditions suggests a conceivable similar concept application for ED, EDR purposes or any other ion-exchange membrane-based technology prone to fouling.

The potential of the RED Fouling Monitor is further aligned with the stated potential field of application of the MFS [15]. Different pre-treatment schemes put in series to the RED Fouling Monitor may give insights about their antifouling efficiency and the ultimate applicability for RED purposes (Fig. 7c). Contrary to pressure-driven membrane processes the dosing of chemical agents, imposing a potential risk for environmental aquatic habitats, is not allowed. Hereby, the potential use of the RED Fouling is restricted to licensed environmentally friendly antifouling agents in accordance to discharge regulations.

Run in parallel to an operational plant or in prior to plant construction, the RED Fouling Monitor can be applied as a tool for fouling prediction and/or detection. As shown with the results, the RED Fouling Monitor was sensitive enough to detect immediate changes attributable to the surrounding media in contact to one side of a single anion-exchange membrane. Furthermore the systems sensitivity is highlighted upon the detection of a relatively small change in both OCV and electrical resistance when exposed to seawater containing an organic foulant (SDBS). This sensitivity may be used for an early detection of fouling, which can result in an early implementation of antifouling measures (pre-treatment, reasonable mechanical or chemical cleaning methods) for a more cost- and energy- efficient fouling management (Fig. 7d). Moreover, the RED Fouling Monitor could potentially be used for identifying the fouling potential of different feed water sources and seasonal changes (Fig. 7e). In this context the RED Fouling Monitor can help to identify constructional locations with feed stream less susceptible towards fouling and give insights on required antifouling measures to be implemented in the plant design. This knowledge can be helpful for the constructional and cost related planning for a RED plant.

4. Conclusions

From the work presented in this paper the following conclusions can be made. The RED Fouling Monitor:

- can be used to distinguish and break down RED fouling into four different fouling constellations, in which one side of a single ion exchange membrane (AEM or CEM) is exposed to a single feed containing foulant(s) (sea- or river water);
- is functional because of the flow-through salt bridge and incorporated reference electrodes positioned in close proximity to the membrane surface;
- shows a stable operation under un-fouled conditions;
- enables to follow the time-resolved progression of fouling relevant operational performance parameters;
- is applicable under both OCV and current conditions;
- gives insights about the effect of current density and the current field direction upon the fouling behavior;
- can give distinctive insights on ohmic and non-ohmic resistances;
- and the concept behind it could be used for further ion-exchange membrane-based systems prone to fouling;
- can be used for a fouling-constellation specific analysis of ion-exchange-membrane coupons;
- is applicable for a broad variety of application fields, including the application for a systematic fouling study to reveal operational and configurational systems less susceptible towards fouling, the testing of pre-treatment and environmental compatible cleaning techniques, the investigation of the fouling potential of different feed streams and due to its sensitivity as an early fouling detection or

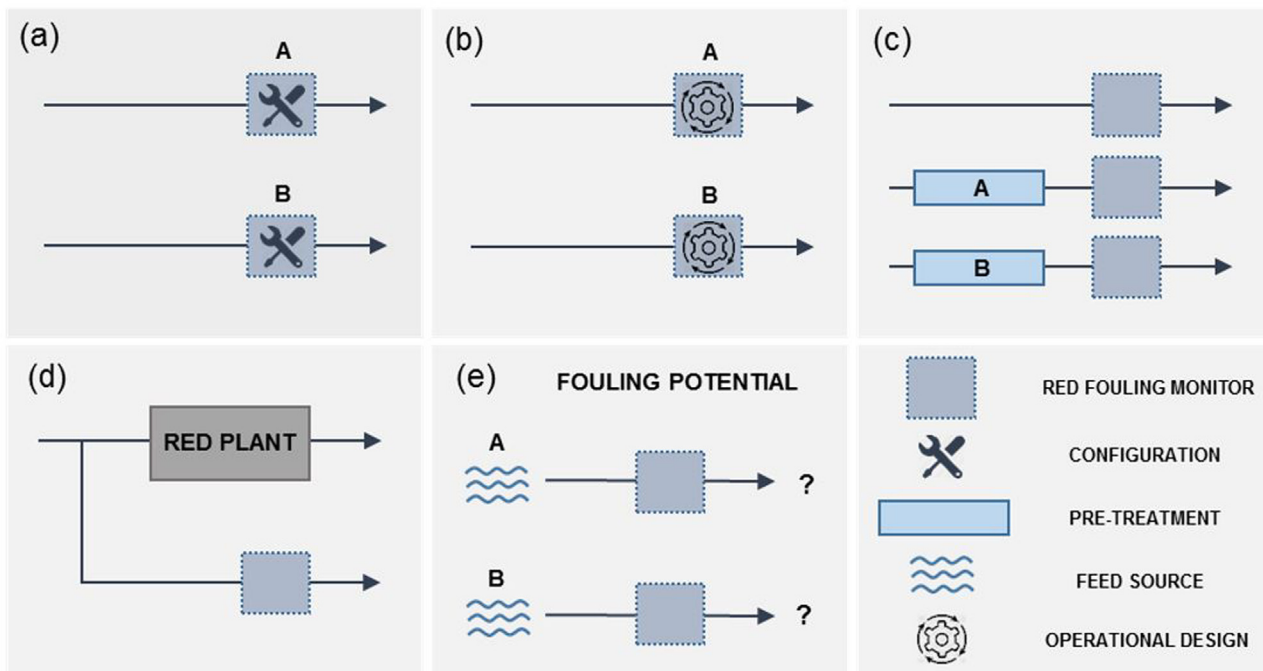


Fig. 7. Fields of potential application for the RED Fouling Monitor, (a) systematic, distinctive fouling analysis and evaluation of different configurational designs, (b) investigation of suitable operational designs including hybrid cleaning and antifouling system, (c) evaluation of pre-treatment schemes, (d) early-stage fouling detection and warning system (e) fouling potential of different feed streams and seasons.

warning system.

Acknowledgements

This work was performed in the cooperation framework of Wetsus, European Centre of Excellence for Sustainable Water Technology (www.wetsus.eu). Wetsus is co-funded by the Dutch Ministry of Economic Affairs and Ministry of Infrastructure and Environment, the Province of Fryslân, and the Northern Netherlands Provinces. This project has also received funding from the European Union's Horizon 2020 research and innovation programme under the Marie Skłodowska-Curie grant agreement No 665874. The authors like to thank the participants of the research theme “Blue Energy” for their input and suggestions and their financial support.

References

- [1] David A. Vermaas, Enver Güler, Michel Saakes, Kitty Nijmeijer, Theoretical power density from salinity gradients using reverse electro dialysis, *Energy Procedia* 20 (2012) 170–184.
- [2] J. Veerman, M. Saakes, S.J. Metz, G.J. Harmsen, Electrical power from sea and river water by reverse electro dialysis: a first step from the laboratory to a real power plant, *Environ. Sci. Technol.* 44 (2010) 9207–9212.
- [3] R.E. Pattle, Production of electric power by mixing fresh and salt water in the hydroelectric pile, *Nature* 174 (1954) (660–660).
- [4] Wenshan Guo, A mini-review on membrane fouling, *J. Bioresour. Technol.* 122 (2012) 27–34.
- [5] D.A. Vermaas, D. Kunteng, M. Saakes, K. Nijmeijer, Fouling in reverse electro dialysis under natural conditions, *Water Res.* 47 (2013) 1289–1298.
- [6] J. Moreno, N. De Hart, M. Saakes, K. Nijmeijer, CO₂ saturated water as two-phase flow for fouling control in reverse electro dialysis, *Water Res.* 125 (2017) 23–31.
- [7] M. Tedesco, H.V.M. Hamelers, P.M. Biesheuvel, Nernst-Planck transport theory for (reverse) electro dialysis: II. Effect of water transport through ion-exchange membranes, *J. Membr. Sci.* 531 (2017) 172–182.
- [8] Aamer Ali, Ramato Ashu Tufa, Francesca Macedonio, Efreem Curcio, Enrico Drioli, Membrane technology in renewable-energy-driven desalination, *Renew. Sustain. Energy Rev.* 81 (2018) 1–21.
- [9] Hong-Joo Lee, Comparison of electro dialysis reversal (EDR) and electro deionization reversal (EDIR) for water softening, *Desalin. J. Desalin.* 314 (2013) 43–49.
- [10] Ying Mei, Chuayang Y. Tang, Recent developments and future perspectives of reverse electro dialysis technology: a review, *Desalination* 425 (2018) 156–174.
- [11] Qun Wang, Xueli Gao, Yushan Zhang, Zhaolong He, Zhiyong Ji, Xinyan Wang, Congjie Gao, Hybrid RED/ED system: simultaneous osmotic energy recovery and desalination of high-salinity wastewater, *Desalination* 405 (2017) 59–67.
- [12] A.H. Galama, N.A. Hoog, D.R. Yntema, Method for determining ion exchange membrane resistance for electro dialysis systems, *Desalination* 380 (2016) 1–11.
- [13] Sz.S. Bucs, A.I. Radu, V. Lavric, J.S. Vrouwenvelder, C. Picioreanu, Effect of different commercial feed spacers on biofouling of reverse osmosis membrane systems: a numerical study, *Desalination* 343 (2014) 26–37.
- [14] A. Siddiqui, S. Lehmann, Sz.S. Bucs, M. Fresquet, L. Fel, E.I.E.C. Prest, J. Ogier, C. Schellenberg, M.C.M. van Loosdrecht, J.C. Kruijthof, J.S. Vrouwenvelder, Predicting the impact of feed spacer modification on biofouling by hydraulic characterization and biofouling studies in membrane fouling simulators, *Water Res.* 110 (2017) 281–287.
- [15] J.S. Vrouwenvelder, J.A.M. van Paassen, L.P. Wessels, A.F. van Dam, S.M. Bakker, The membrane fouling simulator: a practical tool for fouling prediction and control, *J. Membr. Sci.* 281 (2006) 316–324.
- [16] Wenyun Wang, Rongqiang Fu, Zhaoming Liu, Haizeng Wang, Low-resistance anti-fouling ion exchange membranes fouled by organic foulants in electro dialysis, *Desalination* 417 (2017) 1–8.
- [17] D.A. Vermaas, M. Saakes, K. Nijmeijer, Double power densities from salinity gradients at reduced intermembrane distance, *Environ. Sci. Technol.* 45 (2011) 7089–7095.
- [18] V. Lindstrand, A.S. Joensuu, G. Sundstroem, Organic fouling of electro dialysis membranes with and without applied voltage, *Desalination* 130 (2000) 73–84.
- [19] V. Lindstrand, G. Sundstroem, A.S. Joensuu, Fouling of electro dialysis membranes by organic substances, *Desalination* 128 (2000b) (2000) 91–102.
- [20] E. Korngold, F. de Koeroesy, R. Rahav, M.F. Taboch, Fouling of anion selective membranes in electro dialysis, *Desalination* 8 (1970) (1970) 195–220.
- [21] D.A. Vermaas, D. Kunteng, J. Veerman, M. Saakes, K. Nijmeijer, Periodic feedwater reversal and air sparging as antifouling strategies in reverse electro dialysis, *Environ. Sci. Technol.* 48 (2014) 3065–3073.
- [22] J. Moreno, E. Slouwerhof, D.A. Vermaas, M. Saakes, K. Nijmeijer, The breathing cell: cyclic intermembrane distance variation in reverse electro dialysis, *Environ. Sci. Technol.* 50 (2016) 11386–11393.
- [23] Viktoria Lindstrand, Ann-Sofi Jönsson, Göran Sundström, Organic fouling of electro dialysis membranes with and without applied voltage, *Desalination* 130 (2000) 73–84.
- [24] Zhaolong He, Xueli Gao, Yushan Zhang, Yuhong Wang, Jian Wang, Revised spacer design to improve hydrodynamics and anti-fouling behavior in reverse electro dialysis processes, *Desalin. Water Treat.* 57 (58) (2016) 28176–28186.
- [25] Maria D. Kennedy, Hyoung K. Chun, Victor A. Quintanilla Yangali, Bas G.J. Heijman, Jan C. Schippers, Natural organic matter (NOM) fouling of ultra-filtration membranes: fractionation of NOM in surface water and characterisation by LC-OCD, *Desalination* 178 (2005) 73–83.